Inorganica Chimica Acta 480 (2018) 47–53

Contents lists available at ScienceDirect

Inorganica Chimica Acta

journal homepage: www.elsevier.com/locate/ica

Research paper

Electrocatalytic proton reduction by thiolate-capped triiron clusters $[Fe_3(CO)_9(\mu_3\text{-}SR)(\mu\text{-}H)]$ (R = ^{i}Pr, ^{t}Bu)

Shishir Ghosh [a,b], Sucharita Basak-Modi [a], Michael G. Richmond [c], Ebbe Nordlander [d], Graeme Hogarth [b,*]

[a] Department of Chemistry, University College London, 20 Gordon Street, London WC1H 0AJ, UK
[b] Department of Chemistry, King's College London, Britannia House, 7 Trinity Street, London SE1 1DB, UK
[c] Department of Chemistry, University of North Texas, 1155 Union Circle, Box 305070, Denton, TX 76203, USA
[d] Inorganic Chemistry Research Group, Chemical Physics, Center for Chemistry and Chemical Engineering, Lund University, Box 124, SE-221 00 Lund, Sweden

ARTICLE INFO

Article history:
Received 25 January 2018
Received in revised form 10 April 2018
Accepted 18 April 2018
Available online 30 April 2018

Keywords:
Triiron clusters
Thiolate
Electrocatalytic proton reduction
DFT studies

ABSTRACT

The redox behaviour and electrocatalytic proton reduction ability of the thiolate-capped triiron clusters $[Fe_3(CO)_9(\mu_3\text{-}SR)(\mu\text{-}H)]$ (**1**, R = ^{i}Pr; **2**, R = ^{t}Bu) have been investigated. In CH_2Cl_2, both show a quasi-reversible reduction and an irreversible oxidation. The thiol substituent has a significant influence on their reduction potentials ($E_{1/2}$ = −1.24 V for **1** and $E_{1/2}$ = −1.40 V for **2** *vs.* Fc^+/Fc) but less impact on oxidation potentials ($E_{1/2}$ = 0.99 V for **1** and $E_{1/2}$ = 0.93 V for **2** *vs.* Fc^+/Fc). Reduction is quasi-reversible and DFT studies reveal that this is due to scission of an iron-iron bond. While the clusters are not protonated by CF_3CO_2H or $HBF_4{\cdot}Et_2O$, they can catalyse proton reduction of these acids at their corresponding reduction potentials following an ECEC mechanism.

1. Introduction

Development of iron-based electrocatalysts for H_2 evolution is almost entirely centred on diiron complexes that are structural mimics of the active site(s) of [FeFe]-hydrogenase enzymes [1–5]. In contrast, the proton reduction ability of non-enzyme-related iron complexes has been relatively neglected even though the first report of electrocatalytic proton reduction by an iron complex was by [(TPP)Fe(Cl)] (TPP = tetraphenylporphyrin), which catalyses proton reduction at reasonable catalytic rates [6]. Recently, other mononuclear iron catalysts have been developed by several groups, [7–15] some of which are able to catalyse proton reduction more efficiently than the majority of diiron biomimics [15].

Low-valent iron clusters have attracted attention as potential electrocatalysts due to the delocalized nature of bonding in the cluster core that can lead to low reduction potentials and stable reduced species [16–27]. Thus we and others have reported electrocatalytic proton reduction by the tetrairon nitrido-, carbido- and oxo-clusters $[NEt_4][Fe_4(CO)_{12}(\mu_4\text{-}N)]$ [16,17], $[NEt_4]_2[Fe_4(CO)_{12}(\mu_4\text{-}C)]$ [17] and $[Fe_4(CO)_{10}(\kappa^2\text{-dppn})(\mu_4\text{-}O)]$ [18], respectively, which show moderate catalytic activity in organic solvents with their sodium salts also being able to operate in water [17]. Recently, we also reported electrocatalytic reduction of protons by triiron clusters containing a 2-aminopyridinate or 2-aminopyrimidinate ligand [28]. In addition, the sulfido-capped triiron cluster $[Fe_3(CO)_9(\mu_3\text{-}S)_2]$ [19,20] and the diphosphine derivatives, $[Fe_3(CO)_5(\kappa^2\text{-dppv})_2(\mu_3\text{-}S)_2]$ [21] (dppv = 1,2-bis(diphenylphosphino)ethylene) and $[Fe_3(CO)_7(\mu\text{-dppm})(\mu_3\text{-}S)_2]$ [22] (dppm = bis(diphenylphosphino)methane), have also been studied as proton reduction catalysts (Chart 1). The parent cluster $[Fe_3(CO)_9(\mu_3\text{-}S)_2]$ is not readily protonated even by strong acids but is catalytically active for hydrogen production at its second reduction potential in the presence of acetic acid [20], and at its first reduction potential in presence of $HBF_4{\cdot}Et_2O$ [19]. The diphosphine derivative $[Fe_3(CO)_5(\kappa^2\text{-dppv})_2(\mu_3\text{-}S)_2]$, with a more electron-rich cluster core, is protonated by strong acids such as $HBF_4{\cdot}Et_2O$ and displays catalysis initiated by protonation [21]. Recently, we have also investigated the selenide- and telluride-analogues of $[Fe_3(CO)_9(\mu_3\text{-}S)_2]$ (Chart 1) and found that the nature of the chalcogenide exerts a significant influence on their redox response and electrochemical properties [23].

Low-valent thiolate-capped triiron clusters are thus potential candidates as electrocatalytic proton reduction catalysts. A number of such triiron clusters have been reported [29–33] and as part of a preliminary study we have tested two of these, namely $[Fe_3(CO)_9(\mu_3\text{-}S^{i}Pr)(\mu\text{-}H)]$ (**1**) and $[Fe_3(CO)_9(\mu_3\text{-}S^{t}Bu)(\mu\text{-}H)]$ (**2**), as electrocatalysts. Both clusters are capable of reducing protons in their monoanionic state and DFT calculations have been carried out in

* Corresponding author.
E-mail address: graeme.hogarth@kcl.ac.uk (G. Hogarth).

https://doi.org/10.1016/j.ica.2018.04.034
0020-1693/

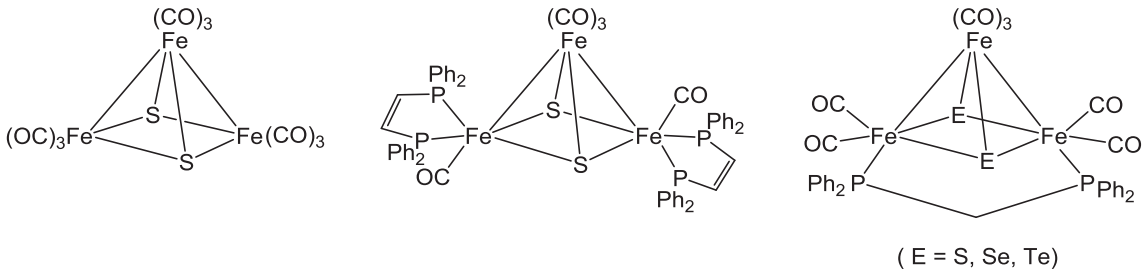

Chart 1. Chalcogenide-capped triiron clusters tested as proton reduction catalysts [19–23].

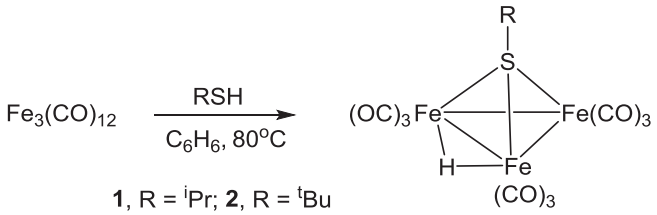

Scheme 1. Synthesis of $[Fe_3(CO)_9(\mu_3\text{-}S^iPr)(\mu\text{-}H)]$ (**1**) and $[Fe_3(CO)_9(\mu_3\text{-}S^tBu)(\mu\text{-}H)]$ (**2**).

order to understand the nature of the key radical anion intermediate in the catalytic process.

2. Results and discussion

2.1. Synthesis and structure of $[Fe_3(CO)_9(\mu_3\text{-}SR)(\mu\text{-}H)]$ (R = ^{i}Pr, ^{t}Bu)

Clusters **1** and **2** were first synthesized by Beer and Haines in 1970 from the direct reaction between equimolar amounts of $[Fe_3(CO)_{12}]$ and RSH (R = ^{i}Pr, ^{t}Bu) at 80 °C (Scheme 1) [29]. Both were characterised by spectroscopic data [29], and later by X-ray crystallography [32,33].

Earlier diffraction data for **1** and **2** were collected at room temperature and we thus collected a low-temperature data set for **1,** an ORTEP diagram generated from the new data is shown in Fig. 1. Although we obtained a different polymorph, metric parameters are similar to those reported earlier by Bau *et. al.* [32]. The molecule consists of an isosceles triangle of iron atoms [Fe(1)—Fe(2) 2.6875(5), Fe(1)—Fe(3) 2.6379(5) and Fe(2)—Fe(3) 2.6366(5) Å] coordinated by nine terminal carbonyls, a face-capping isopropyl thiolate ligand, and an edge-bridging hydride. The carbonyls are evenly distributed among three irons and the thiolate ligand asymmetrically caps one face of the metal triangle [Fe(1)—S(1) 2.1411(7), Fe(2)—S(1) 2.1446(6) and Fe(3)—S(1) 2.1203(7) Å]. The hydride, which was located in a difference map and spans the longest Fe—Fe vector, lies on the opposite face of the metallic plane with respect to the thiolate ligand. The OC—Fe—Fe angles along this particular Fe—Fe edge open up significantly due to the hydride disposition [C(1)—Fe(1)—Fe(2) 105.48(8) and C(4)—Fe(2)—Fe(1) 106.01(9)°] as expected. The ^{1}H NMR spectrum of **1** shows a high-field singlet at −23.76 ppm, consistent with the presence of a bridging hydride, in addition to a septet and a doublet at 4.20 and 1.70 ppm, respectively, with an intensity ratio of 1:6, that are attributed to the methine and methyl protons of the isopropyl thiolate ligand.

2.2. Attempted protonation and electrochemistry

Since protonation is a key step in electrocatalytic proton reduction, clusters **1** and **2** were treated with a range of acids [CH_3CO_2H ($pK_a \approx 22.3$), CF_3CO_2H ($pK_a \approx 12.7$) and $HBF_4{\cdot}Et_2O$ ($pK_a \approx 0.1$)] in

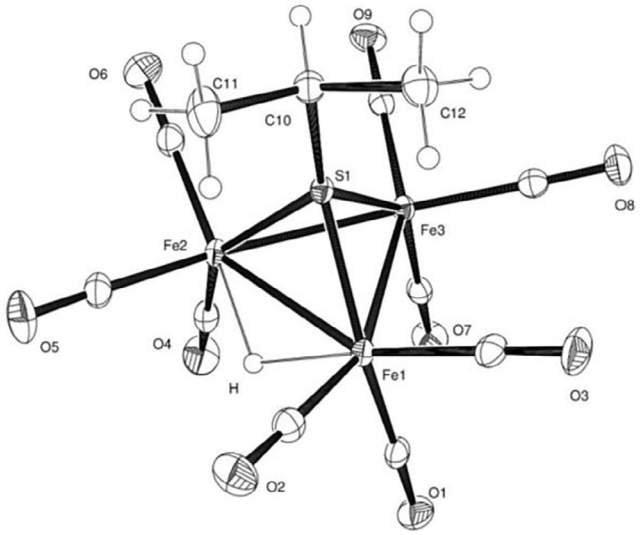

Fig. 1. ORTEP diagram of the molecular structure of $[Fe_3(CO)_9(\mu_3\text{-}S^iPr)(\mu\text{-}H)]$ (**1**). Selected bond distances (Å) and angles (°): Fe(1)—Fe(2) 2.6875(5), Fe(1)—Fe(3) 2.6379(5), Fe(2)—Fe(3) 2.6366(5), Fe(1)—S(1) 2.1411(7), Fe(2)—S(1) 2.1446(6), Fe(3)—S(1) 2.1203(7), Fe(1)—Fe(2)—Fe(3) 59.393(12), Fe(2)—Fe(1)—Fe(3) 59.343(12), Fe(2)—Fe(3)—Fe(1) 61.263(12), Fe(1)—S(1)—Fe(2) 77.67(2), Fe(2)—S(1)—Fe(3) 76.37(2), Fe(3)—S(1)—Fe(1) 76.49(2), S(1)—Fe(1)—Fe(2) 51.224(17), S(1)—Fe(1)—Fe(3) 51.401(18), S(1)—Fe(2)—Fe(1) 51.108(19), C(1)—Fe(1)—Fe(2) 105.48(8), C(4)—Fe(2)—Fe(1) 106.01(9), C(2)—Fe(1)—Fe(2) 102.28(8), C(5)—Fe(2)—Fe(1) 101.85(8).

CH_2Cl_2 [34]. Infrared spectroscopy shows that the clusters do not react with these acids and are stable in acidic solutions. The electrochemical responses of **1** and **2** were next examined by cyclic voltammetry in CH_2Cl_2, and the cyclic voltammograms (CVs) recorded at a scan rate of 0.1 V/s are shown in Fig. 2. Both clusters display a quasi-reversible reduction wave together with a relatively large irreversible oxidative wave. The reversibility of the reductive process of both clusters improves with scan rate, while the oxidative process remains irreversible at all scan rates (0.025 –1 V/s) (Figs. S1 and S2). A plot of reductive peak currents against the square root of scan rates indicates that the reductive feature of both clusters originates from a diffusion-controlled process (Fig. S3). The dependence of the current on the scan rate (v) ($i_p/\sqrt{v}$) (Fig. S4) associated with the $0/1^-$ wave for both clusters shows slight deviations from linearity only at very slow scan rates, which indicates that the electrode process tends towards a two-electron transfer on longer time scales.

The reduction potential of **2** shows a 160 mV negative shift due to the presence of an additional methyl group on the thiolate ligand ($E_{1/2} = -1.24$ V for **1** and $E_{1/2} = -1.40$ V for **2**), but this has little effect on the oxidation potential ($E_{1/2} = 0.99$ V for **1** and $E_{1/2} = 0.93$ V for **2**). The peak current of the anodic wave of the reductive process observed on the return scan at scan rate 0.1 V/s is *ca.* 50% compared to that of the cathodic wave on